J Nanostruct 15(2): 666-683, Spring 2025

RESEARCH PAPER

Synthesis and Characterization of Cerium, Nitrogen, and co-doped TiO_2 Photoanodes for Dye-Sensitized Solar Cells

Javad Mohammadian [1], ***Amir Masoud Arabi*** [2*], ***Hamid Haratizadeh*** [1*], ***Mozhgan Hosseinnezhad*** [3], ***Kamaladin Gharanjig*** [3]

[1] *Department of Physics, Shahrood University of Technology, University Blvd, 3619995161 Shahrood, Iran*

[2] *Department of Inorganic Pigments and Glazes, Institute for Color Science and Technology (ICST), Tehran, Iran*

[3] *Department of Organic Colorants, Institute for Color Science and Technology (ICST), Tehran, Iran*

ARTICLE INFO

Article History:
Received 09 January 2025
Accepted 24 March 2025
Published 01 April 2025

Keywords:
Anatase TiO_2 phase
Ce and N co-doped TiO_2
Dye-Sensitized Solar Cells (DSSC)
Photovoltaic properties
Sol-gel

ABSTRACT

Cerium (Ce), nitrogen (N), and their co-doped TiO_2 nanoparticles were produced through a cost-effective sol-gel process. Samples produced were analyzed using various analysis techniques. Structural studies revealed that pure TiO_2, 3 mol% Ce-doped TiO_2, and 5 mol% Ce-doped TiO_2 show anatase TiO_2 structure, except for 7 mol% Ce-doped TiO_2 and 10 mol% Ce-doped TiO_2 which have semi-crystalline nature. Energy dispersive X-ray spectroscopy (EDS) results confirmed the presence of the stoichiometric ratio Ce, Ti, and O. According to the Kubelka-Munk model, the E_{gap} value for pure TiO_2 decreases with Ce content from 3.61 eV to 3.48 eV. The photoluminescence spectroscopy (PLS) analysis was performed to investigate the electron-hole recombination in both pure TiO_2 and Ce-doped TiO_2. After complete examination of the physicochemical properties of the synthesized Ce-doped TiO_2, photovoltaic cells were assembled to compare the effects of the optimized cerium doped, nitrogen doped, and co-doped samples. In Ce-doped solar cells, 5 mol% Ce-doped TiO_2 showed the highest efficiency, with a 26% improvement over the undoped sample. Nitrogen doping also enhanced the efficiency by 22%. To explore the synergistic effect, co-doping with both cerium and nitrogen was implemented. Remarkably, the co-doped cell exhibited a 46% increase in efficiency. Typical Nyquist plot obtained for the DSSC under open-circuit voltage (V_{OC}) condition indicated low resistance to charge recombination for 5 mol% Ce-doped TiO_2 sample with R_s of 23.14 Ω, R1 of 4.61 Ω, and R2 of 13.84 Ω and the longest electron lifetime of 15.23 ms, suggesting an increasing trend in V_{OC} and a decreasing trend in recombination rate.

How to cite this article
Mohammadian J., Arabi A., Haratizadeh H., Hossein Nejad M., Gharanjig K. Synthesis and Characterization of Cerium, Nitrogen, and co-doped TiO_2 Photoanodes for Dye-Sensitized Solar Cells. J Nanostruct, 2025; 15(2):666-683. DOI: 10.22052/JNS.2025.02.026

INTRODUCTION

The rapid and extensive use of fossil fuels, coupled with the negligent implementation of environmental regulations, has brought our planet to the brink of destruction [1]. This has compelled humanity to seek environmentally benign alternatives [2]. Renewable energy sources

---

* *Corresponding Author Email: aarabi@icrc.ac.ir*
Hamid.haratizadeh@gmail.com

are widely recognized as the most effective means of mitigating the large-scale exploitation of fossil fuels, a primary driver of flooding, global warming, and air pollution [3]. To address these pressing issues, there is an urgent need for cost-effective and proficient photovoltaic devices that can harness solar energy and convert it into electricity. The third generation of photovoltaic technology, i.e., Dye-sensitized solar cell (DSSC), has emerged as a promising solution. The first DSSC was developed in 1991 through the pioneering work of Grätzel and O'Regan [4]. Following silicon-based solar cells, DSSCs have gained significant prominence in photovoltaic technology because of their inherent advantages including environmental friendliness and low cost. Fundamentally, a DSSC comprises four key components: the photoanode, the sensitizer, the redox couple, and the counter electrode. A major obstacle hindering the attainment of higher power conversion efficiency (PCE) is interfacial recombination between the fluorine-doped tin oxide (FTO), the sensitizer, and the photoanode [5]. Furthermore, while dye absorption spans a wide wavelength range, leading to the generation of electrons with varying energy levels, only those electrons that possess energies equal to or less than the bandgap of the photoanode can participate in the charge transfer process [6].

Anatase titanium dioxide (TiO_2) serves as a widely utilized photoanode material for manufacturing DSSCs, primarily attributed to its simultaneous visible light and ultraviolet absorption capability. In addition, its energy bandgap is 3.2 eV with an acceptable electron mobility of 0.4 cm^2/Vs, contributing to its chemical stability, high conversion efficiency, non-toxicity, and low cost [6, 7].

When sunlight photons strike the solar cell, electrons located in the dye's highest occupied molecular orbital (HOMO) become excited and are promoted to its lowest unoccupied molecular orbital (LUMO). Following this excitation, the electrons are transferred to the conduction band of TiO_2, a process driven by the energy alignment, as the conduction band of TiO_2 is positioned at a lower energy level than the dye's LUMO. This electron transfer process highly influences the efficiency of the solar cell, as photocurrent exhibits a direct proportionality to the number of electrons transferred. One of the key factors that diminishes the DSSC efficiency is the charge carrier recombination. Specifically, the elevated electron from the dye to the conduction band of the semiconductor recombines with the holes in the electrolyte. This phenomenon is commonly referred to as dark current. In this context, the photoanode assumes a crucial role in facilitating the efficient separation and transport of electrons towards the external contact (i.e., the FTO) [9]. Consequently, the overall PCE is adversely affected by factors such as electron-hole recombination, limited light harvesting efficiency, sluggish electron transfer rates within the photoanode, and dark current [10]. To mitigate these electron losses, researchers have investigated a diverse range of strategies, encompassing the synthesis of semiconductors with distinct morphologies [8], the utilization of semiconductor composites [7–9], and the doping of semiconductors with metallic or non-metallic atoms [14-17].

Doping, a relatively straightforward technique, offers a means for modifying the physical and optical properties of materials. Even with the incorporation of minute amounts of dopant, significant enhancements in PCE can be achieved. To ensure optimal dopant selection for TiO_2, it is crucial to minimize the disparity between the ionic radius of the Ti^{4+} ion and that of the dopant, thereby preventing lattice distortion [5].

Doping TiO_2 with lanthanide elements, such as Pr, Eu, Fe, Ce, Nd, and Yb, and their corresponding oxides, has been shown to increase the separation of electron-hole and its visible light absorption [18]. This visible light activity is crucial from an energy perspective [19]. In addition, previous studies have reported a delay in the recombination of electron-hole in TiO_2 nanostructures. From the lanthanides group, cerium oxides show appropriate catalytic and optical properties, along with redox potential for Ce^{4+}/Ce^{3+} couple [20]. Ce doping in TiO_2 not only red-shifts the absorption spectra but inhibits the phase transformation from anatase to rutile [20]. Cerium ions (Ce^{4+}/Ce^{3+}) are unique p-type semiconductors characterized by a wide band gap, multiple electron energy levels, and variable valence states [21]. The partially filled f-orbitals of cerium impart distinctive properties to TiO_2. They can reduce the band gap energy of TiO_2 by introducing impurity states below the conduction band, even at low doping concentrations (<1%) [22].

Furthermore, doping TiO_2 with non-metals, for example N [23, 24], C [25], B [26], S [27] and F [28, 29], has been demonstrated to narrow the bandgap and enhance light absorption in the visible region. While numerous studies have investigated TiO_2 doping with either transition metals or non-metals individually, there are limited research studies exploring the combined effects of these dopants in TiO_2 for photovoltaic applications [30]. In this study, we doped TiO_2 with Ce as a transition metal and N as a non-metal for improving photovoltaic performance. The influence of the Ce/N co-doped TiO_2 photoanodes on the photovoltaic properties of DSSCs has been also examined.

Numerous approaches such as electrochemical, hydrothermal, sonochemical, microwave, and sol-gel methods can be applied for synthesizing and modifying TiO_2. The sol-gel technique is particularly notable among these methods owing to its straightforward approach and its capacity to achieve precise regulation of crystallite size, surface area, phase composition, and morphology [31].

This research investigates doping of cerium into TiO_2 nanopowder and its effect on the physical characteristics of the material and the electrical behavior of DSSCs. For this purpose, Ce-doped TiO_2 (TC) nanopowders were synthesized via sol-gel method. Their optical properties, structure, electrical properties, and dynamics were analyzed through various analytical techniques. After that, photovoltaic cells were assembled using Ce-doped, N-doped, and their co-doped TiO_2 to evaluate the photovoltaic properties of the cells.

MATERIALS AND METHODS

Cerium-doped TiO_2 ($Ce_xTi_{1-x}O_2$) nanopowders were prepared by the sol-gel technique. The starting reagent materials were cerium (III) nitrate hexahydrate ($Ce(NO_3)_3.6H_2O$, Aldrich), titanium tetra-isopropoxide (TTIP, ≥97.0%, Sigma Aldrich), acetic acid (99%, Sigma Aldrich), ethyl alcohol (95.0%, Sigma Aldrich), isopropyl alcohol (IPA, ≥98%, Sigma Aldrich), PEG (Poly ethylene glycol, Aldrich), and distilled water (DI).

Synthesis of pure TiO_2 and Ce-doped TiO_2 nanopowders by sol-gel process

In a typical procedure, a mixture of 3.2 mL of TTIP and 9.5 mL of IPA was prepared under stirring for 1 hour, followed by the addition of 24 mL ethyl alcohol and 10 mL acetic acid. The mixture was stirred for another 1.5 hours to ensure homogeneity. The color of mixture changed from transparent to white after the addition of acetic acid. After drying the obtained products in an oven at 90°C for 12 hours, calcination was performed at 450 °C for 4 hours to achieve a homogenous particle size [32,33]. Ce-doped TiO_2 powders with varying Ce concentrations of 3-10 mol% (TC3-10) were synthesized and labeled according to Table 1.

TiO_2 paste preparation

TiO_2 pastes were prepared by using the TC0 and TC3-10 nanopowders. First, the synthesized TiO_2 powder was heated up to 400°C for 30 min to remove the absorbed moisture and organic impurities. Then, 1g of the powder was mixed with 2ml of PEG (Poly ethylene glycol) and 4ml of ethanol using magnetic stirring at 300 rpm to obtain a homogenous and viscous mixture. This paste was then used for TiO_2 doctor blade printing on FTO substrates.

Characterization

Optical properties of the TC0 and the TC3-10 nanoparticles were obtained using diffuse reflection spectroscopy (DRS) with an S-4100 SCINCO spectrophotometer, while photoluminescence (PL) spectra were recorded on a Perkin-Elmer spectrophotometer. The crystalline structure of the synthesized TiO_2 and TC3-10 nanoparticles were studied using an X’Pert PRO MPD X-ray powder diffractometer (XRD). The bonding environment of all samples was evaluated through Fourier-transform infrared spectroscopy (FTIR) using a Thermo Avatar FTIR system covering a wide range from 4000 to 500 cm^{-1}. Raman shift

Table 1. Sample designation.

Sample	Label
TiO_2-0% Ce	TC0
TiO_2-3% Ce	TC3
TiO_2-5% Ce	TC5
TiO_2-7% Ce	TC7
TiO_2-10% Ce	TC10

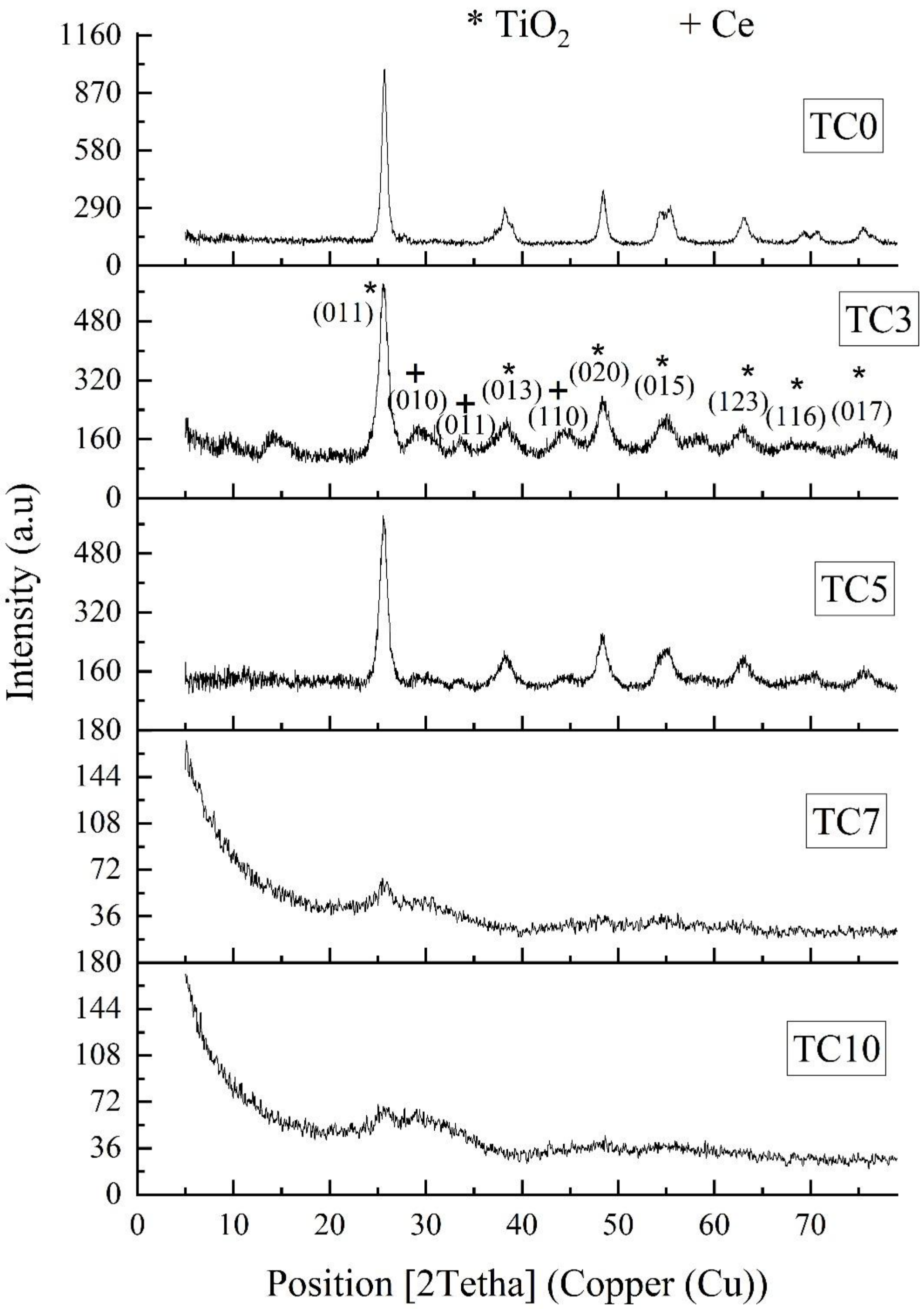

Fig. 1. XRD patterns of pure and Ce-doped TiO_2 samples.

Table 2. Structural parameters of pure and Ce-doped TiO_2 samples.

Sample	Phase	Crystal structure	Lattice parameters	
			Calculated	JCPDS
TC0	Anatase	Tetragonal	a=b=3.7556, c=10.21	a=b=3.7300, c=9.3700
TC3	Anatase	Tetragonal	a=b=3.26, c=10.21	a=b=3.7300, c=9.3700
TC5	Anatase	Tetragonal	a=b=3.7596, c=9.9589	a=b=3.7300, c=9.3700

of the samples was measured in the 100-3500 cm^{-1} range using a confocal Raman spectrometer (Horiba Jobin Yvon HR800) which uses a 632.8 nm laser. The morphology and particle size of the samples were determined using a field emission scanning electron microscope (FESEM, Zeiss Sigma HV 300-S) and an energy dispersive X-ray spectroscopy (EDS, Aztec Oxford) system. The electrical properties were measured under AM1.5 irradiation intensity, which corresponds to a standard solar spectrum. The electron dynamics in the DSSC was examined using electrochemical impedance spectroscopy (EIS, ZVIE 5MP).

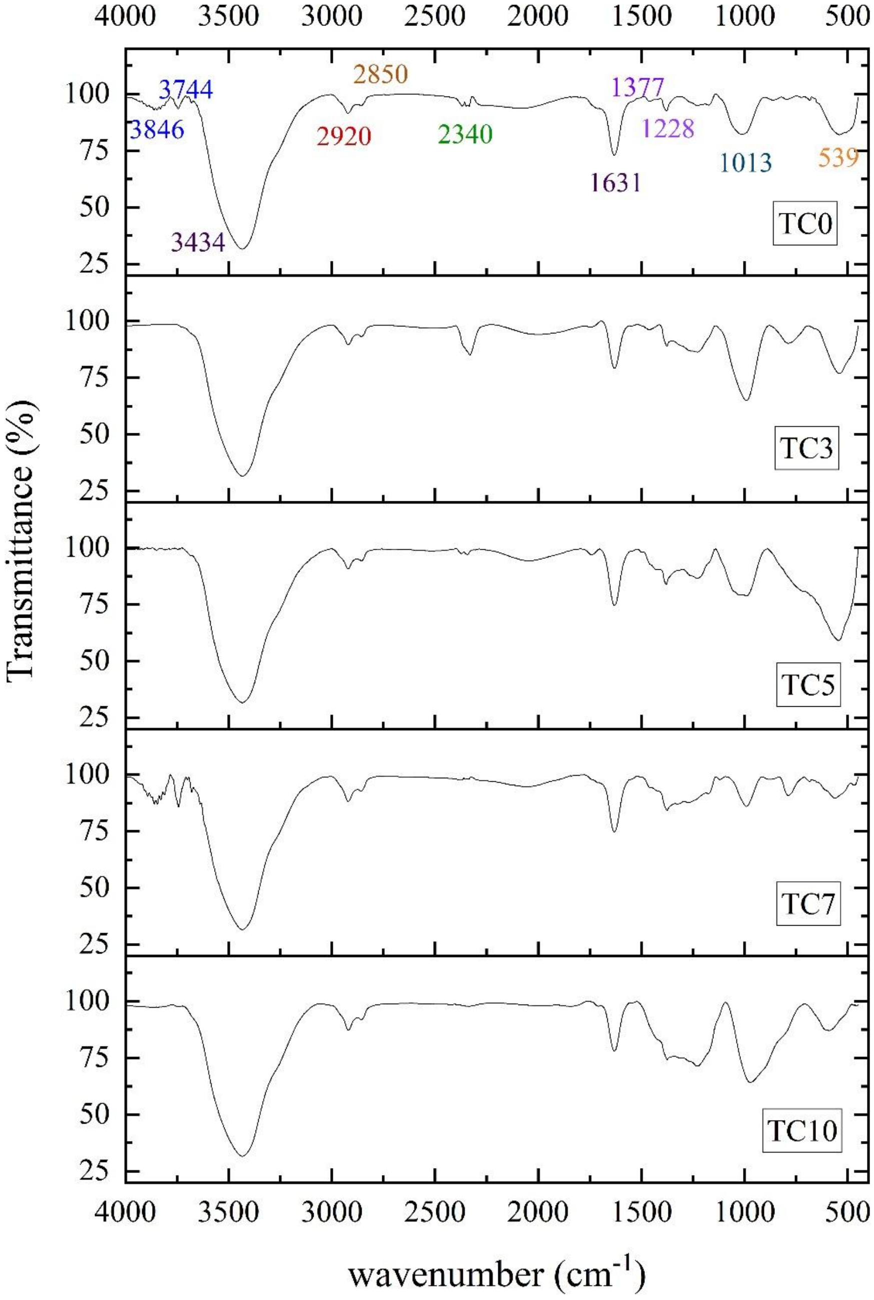

Fig. 2. FTIR analysis of pure and Ce-doped TiO_2 samples.

RESULTS AND DISCUSSION

XRD patterns

Fig. 1 presents XRD patterns obtained for the TC0 and TC3-10 samples. The peaks at 25.68°, 38.28°, 48.43°, 54.38°, 55.39°, 63.10°, 69.33°, 70.62° and 75.61° correspond to (110), (400), (020), (510), (121), (321), (611), (022) and (710) diffraction planes in anatase TiO_2 phase according to JCPDS card No. 96-101- 0943. The introduction of Ce creates extra peaks at 29.17°, 33.44° and 44.95° corresponding to (010), (011) and (110) planes of anatase TiO_2 according to JCPDS card No. 96-900- 8492. Ce-doped TiO_2 exhibited similar peaks but with lower intensity, which have also

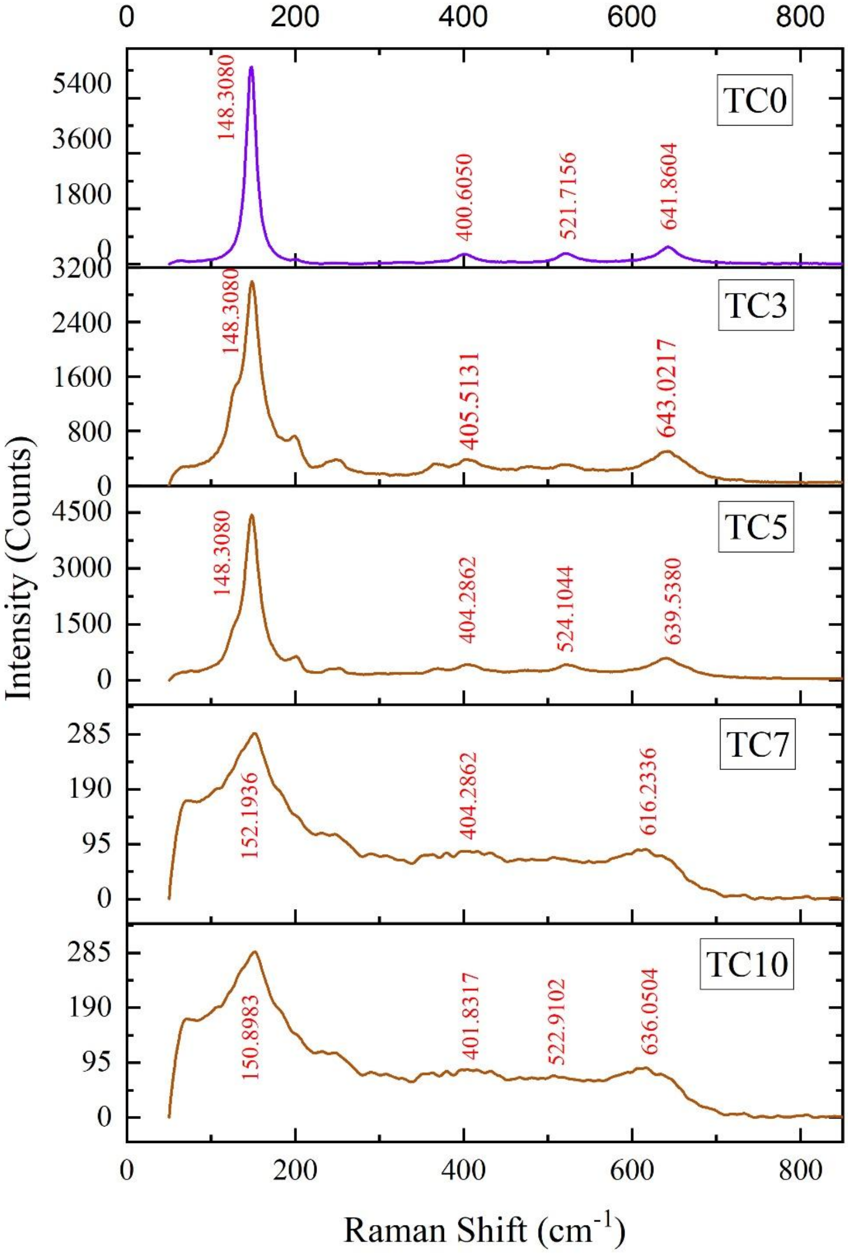

Fig. 3. Raman spectra of pure and Ce-doped TiO_2 samples.

shifted slightly to higher angles mainly due to the interstitial replacement of Ce ions for Ti ions [34]. This doping may suppress the transformation of anatase phase to rutile or brookite [35]. The crystalline size and the lattice parameter are also affected by doping of Ce. Since the ionic radius of Ce^{3+} (1.03 Å) lies between that of Ti^{4+} (0.68 Å) and O^{2-} (1.32 Å), it is more likely that Ce^{3+} occupies interstitial positions [36]. A mixture of phases can be seen for higher Ce contents (TC7 and TC10) [37]. The observed slight shift in the diffraction peaks after Ce doping indicates lattice distortions induced by Ce doping. The structural parameters measured from XRD patterns are summarized in Table 2, confirming the successful synthesis of both TC0 and TC3-10 photoanodes.

FTIR spectra

According to Fig. 2, FTIR spectra confirm the

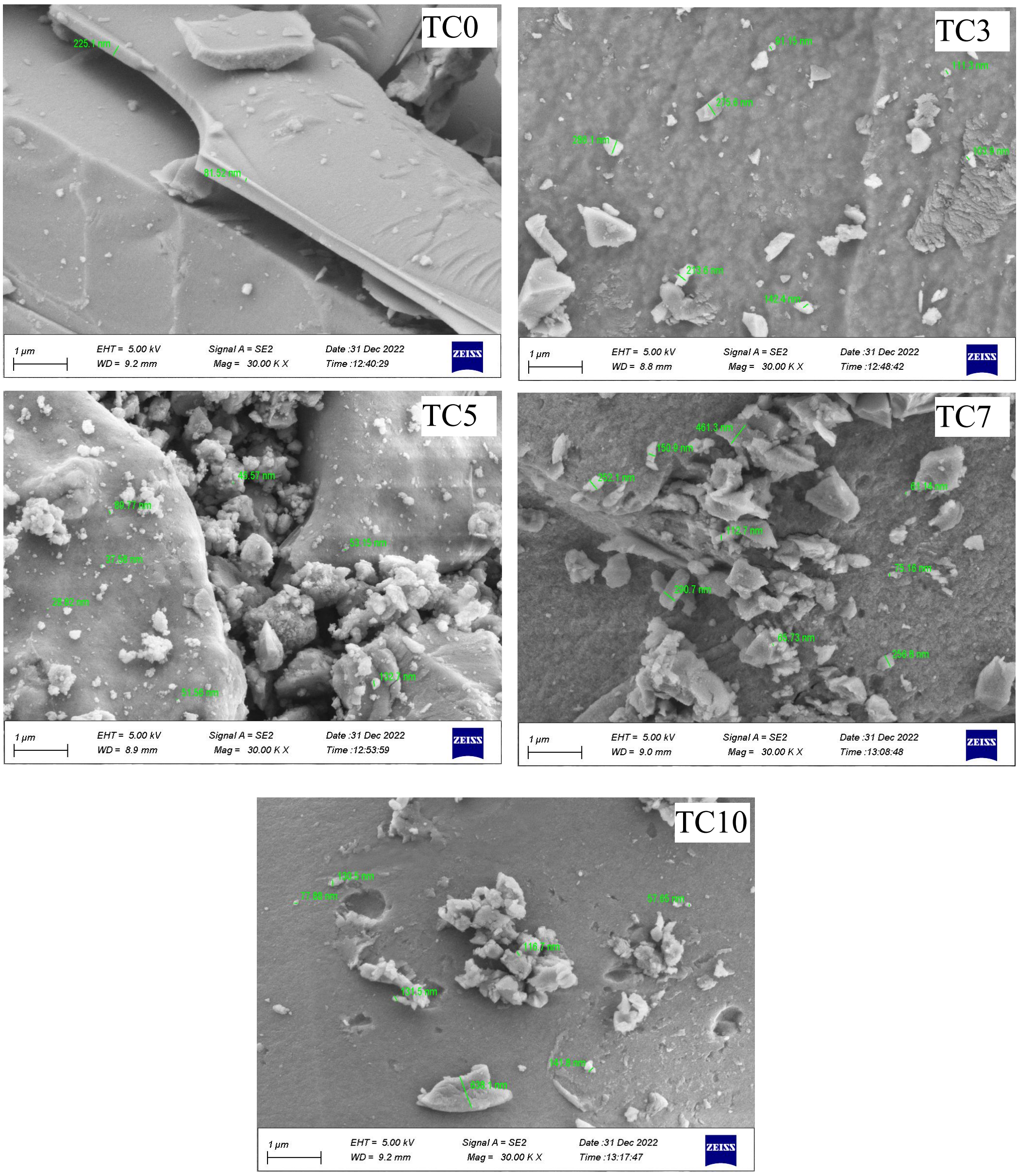

Fig. 4. SEM images of pure and Ce-doped TiO_2 samples.

high purity of the samples. The spectra exhibit weak peaks at 2920 cm^{-1}, 2850 cm^{-1}, and 2340 cm^{-1} associated with the vibration of organic groups such as carboxylate, hydroxyl, and alkane. The peaks corresponding to the stretching vibration of C-H in alkane groups were not completely removed even after washing with ethanol and DI water. The strong peak at 537-561 cm^{-1} represents

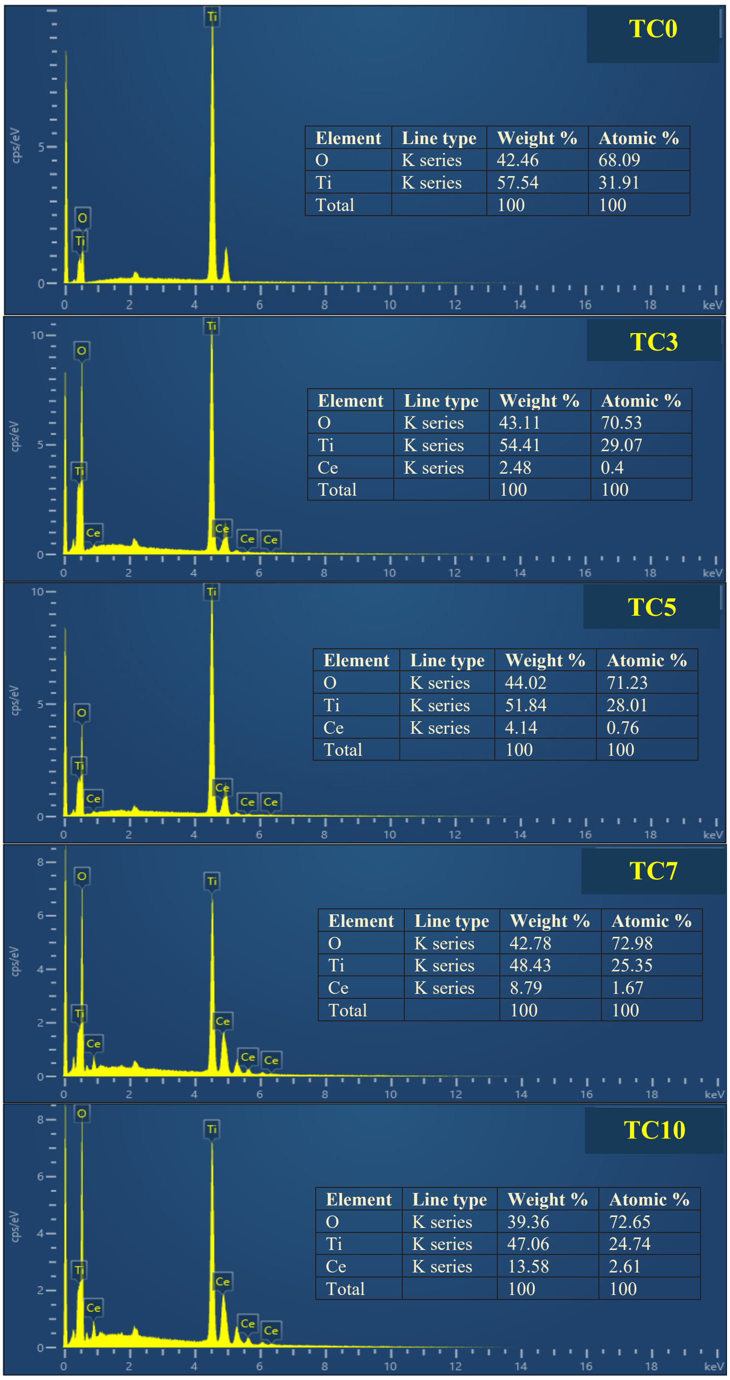

TC0

Element	Line type	Weight %	Atomic %
O	K series	42.46	68.09
Ti	K series	57.54	31.91
Total		100	100

TC3

Element	Line type	Weight %	Atomic %
O	K series	43.11	70.53
Ti	K series	54.41	29.07
Ce	K series	2.48	0.4
Total		100	100

TC5

Element	Line type	Weight %	Atomic %
O	K series	44.02	71.23
Ti	K series	51.84	28.01
Ce	K series	4.14	0.76
Total		100	100

TC7

Element	Line type	Weight %	Atomic %
O	K series	42.78	72.98
Ti	K series	48.43	25.35
Ce	K series	8.79	1.67
Total		100	100

TC10

Element	Line type	Weight %	Atomic %
O	K series	39.36	72.65
Ti	K series	47.06	24.74
Ce	K series	13.58	2.61
Total		100	100

Fig. 5. EDS analysis of pure and Ce-doped TiO_2 samples.

Ti-O and Ce-O bonds [38]. This study indicates that samples are of good quality and are suitable for further characterization.

Raman Spectroscopy

Characteristic peaks of anatase TiO_2 can be observed at 148, 400, 521, and 641 cm^{-1} according to Raman spectra shown in Fig. 3 [39]. In doped TiO_2 samples, these vibrational modes are shifted to higher wavenumbers compared to TC0. Lack of additional Raman bands relating to the dopants, combined with the observed peak shifts, strongly suggests uniform doping and distribution of dopant ions within the titanium sites [40]. The observed shifts in Raman peak positions, reductions in peak intensity, as well as the broadening of the symmetric vibration peak of O-Ti-O are indicative of several events: reduced crystallite size, grain boundary formation, and potential oxygen deficiencies within the TiO_2 lattice [41,42].

FE-SEM and EDS analyses

The morphology of the particles was almost the same irrespective of the Ce content, as shown in FE-SEM images (Fig. 4). Since the particles were agglomerated, mechanical grinding was used for preparing TiO_2 paste. The utilization of nanocrystalline particles in the solar cell enhances electron/hole transfer, thereby avoiding the need for any additives. In addition, the EDS spectra (Fig. 5) confirmed the stoichiometric ratio of Ce, Ti, and O, with no unwanted impurities, confirming the high purity of the doped samples.

Optical properties

DRS analysis

DRS spectra of TC0 and TC3-10 samples at room temperature in the wavelength range of 200-800 nm are shown in Fig. 6. The reduction of diffuse reflectance intensity suggests that the light absorption in the visible spectrum is increased. In the case of TC0, electron transitions between Ti 3d and O 2p states result in optical absorption [43]. It is evident that the absorption bands shift towards higher wavelengths (red shift) after the addition of the Ce dopant. The band gap energy (E_g) of TC0 and TC3-10 samples was determined using Kubelka-Munk plots, as illustrated in Fig. 7. The energy relating to the indirect allowed transition from the valence band (V.B.) maximum to the

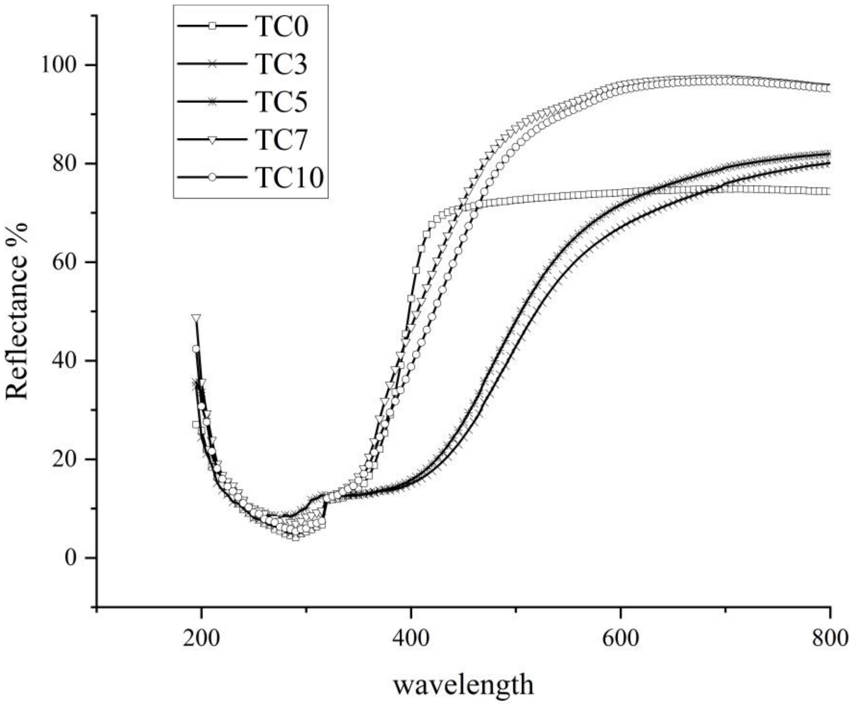

Fig. 6. DRS of pure and Ce-doped TiO_2 samples.

conduction band (C.B.) minimum was determined by linearly extrapolating the plot of (F(Rα)hυ)1/2 as a function of photon energy (hυ) [44]. The calculated E_g for TC0, TC3, TC5, TC7, and TC10 samples are 3.61 eV, 3.57 eV, 3.48 eV, 3.89 eV, and 3.97 eV, respectively.

The incorporation of impurities or the presence of vacancy defects within the band gap (between the V.B. and C.B.) of TiO_2 can lead to modifications in its bandgap energy [45]. These changes provide sites for cerium doping, leading to the creation of intermediate energy levels associated with the Ce 4f states within the TiO_2 bandgap. This phenomenon can significantly influence the photocatalytic and electrocatalytic activities of the material [46,47]. The E_g of TC0 is 3.61 eV, which reduces to 3.48 eV upon increasing the Ce content to 5 mol% (TC5 sample). Researchers have reported that the creation of electron-hole pairs under the exposure of visible light is significantly facilitated in the presence of Ce 4f levels [48,49].

PL analysis

Photoluminescence (PL) test was employed to investigate electron-hole pair recombination in TC0 and TC3-10 samples, as depicted in Fig. 8. All samples exhibited a similar PL behavior. This similarity in PL signals is often observed because of the half- or fully-filled outer electron configuration of the dopant in its stable chemical state [50]. In the case of TC3-10, the electron configuration of the filled outer shell of Ce^{4+} ([Xe] $4f^0$ $5d^0$ $6s^0$) does not significantly alter the spectral shape. The PL spectra of all samples displayed a broad and intense emission band in the 350-450 nm range upon excitation at 254 nm, which can be attributed to excitonic luminescence [51]. A prominent peak observed around 400 nm is associated with radiative transitions between bands involving photoexcited electrons [52]. Additionally, the band at 464 nm is characteristic of rutile TiO_2 [53]. Despite the similar spectral shapes, the PL intensity changed considerably, mainly due to the existence of oxygen vacancies and surface defects, which in turn are dependent on the ability of the dopant to capture electrons [50]. With increasing the Ce content, the formation of Ti-O-Ce bonds reduces the concentration of oxygen vacancies, hence decreasing the PL intensity [52].

Studies have shown that surface defects and oxygen vacancies are not capable of binding electrons for the formation of excitons. Instead,

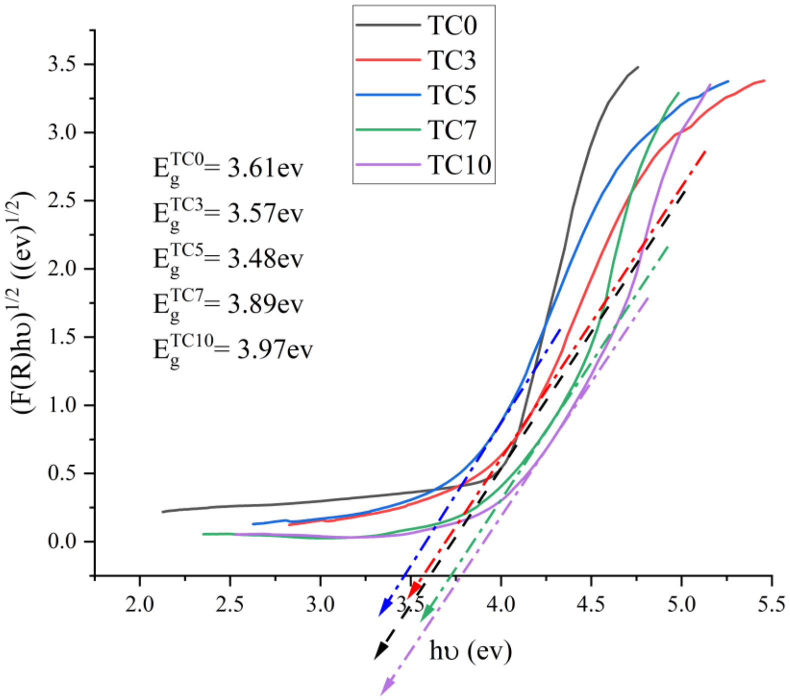

Fig. 7. Kubelka-Munk function and band gap energy of pure and Ce-doped TiO_2 samples.

they are captured by Ce^{4+} ions, resulting in the reduction of Ce^{4+} to Ce^{3+} [50], and hence a decrease in PL intensity. The lower PL intensity is often associated with reduced recombination of photogenerated charges [54]. This observation suggests that increasing the Ce content can decrease the recombination rate of electron-hole pairs, thereby enhancing the potential for improved photovoltaic properties.

Photovoltaic properties

Current density (J) as a function of voltage (V) and the power measurements of the DSSCs fabricated based on TC0 and TC3-10 samples are shown in Fig. 9 and Fig. 10, respectively, to clarify the effect of Ce doping on the photovoltaic performance of DSSCs. The tests were conducted by using a sun simulator under AM1.5 standard condition. Table 3 lists the associated photovoltaic parameters for these measurements. According to Fig. 9, the incident photoelectric conversion efficiency (IPCE) is as follows: TC5 > TC3 > TC0 > TC7 > TC10. Because of the impact of Ce doping, TC5 has 29% more efficiency than TC0 with short circuit current density (J_{SC}) of 10.3 mA/cm^2, open circuit voltage (V_{OC}) of 545 mv, energy conversion efficiency (η) of 5.613%, and fill factor (FF) of 47.4%. The greater electron density is a result of improved photo-injection and effective photoexcitation in TiO_2. Table 4 compares the results of this investigation

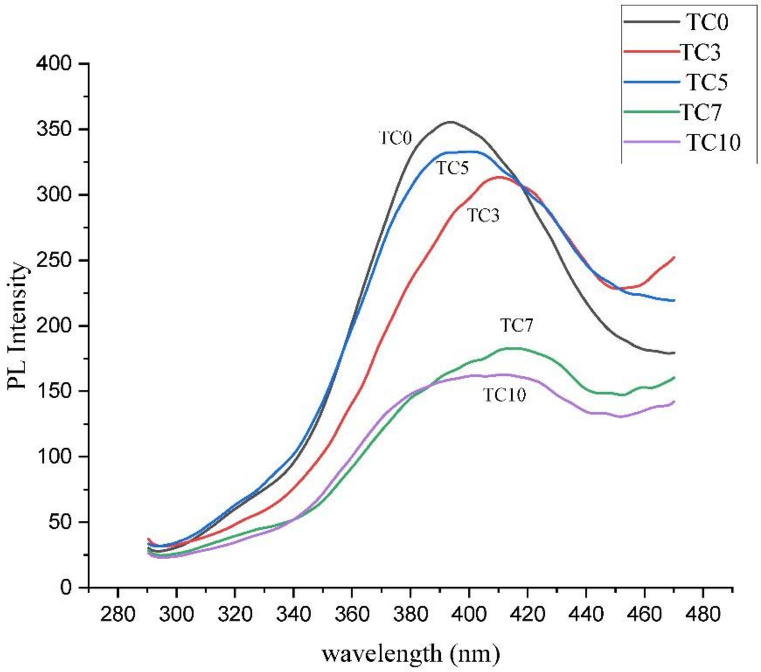

Fig. 8. PL spectra of pure and Ce-doped TiO_2 samples.

Table 3. Electrical properties of TC0 and TC3-10 samples.

Photoanodes	E_g (ev)	J_{SC} (mA/cm^2)	V_{OC} (V)	η (%)	FF (%)
TC0	3.61	9.02	0.493	4.45	43
TC3	3.57	10.1	0.515	5.202	47
TC5	3.48	10.30	0.545	5.613	47.4
TC7	3.73	8.32	0.514	4.277	43.3
TC10	3.76	7.95	0.529	4.206	34.4

with previously reported studies.

The electrical properties of nitrogen-doped TiO_2 samples (TN3, TN5, and TN7) and Ce and N co-doped TiO_2 samples (TN3C5, TN5C5, and TN7C5) were also investigated and compared with those of the TC5 sample, as shown in Fig. 11 and Fig. 12. The corresponding photovoltaic parameters of these samples are listed in Table 5. DSSCs employing the co-doped TiO_2 exhibit significantly enhanced energy conversion efficiency (6.51) and fill factor (67.4) compared to TC0 (η =4.45, FF=43) and TC5 (η=5.613, FF=47.4). While nitrogen doping also enhanced efficiency by 22%, cerium doping proved to be more beneficial. Remarkably, the co-doped cell exhibited a 46% increase in efficiency. The fill factor followed a similar trend, reaching 47.4% for the optimized cerium-doped cell (TC5), 64.5% for the optimized nitrogen-doped cell (TN5), and an impressive 67.4% for the co-doped cell (TN3C5), confirming the positive interplay between cerium and nitrogen doping. The increased electric current towards the cathode is likely attributed to the introduction of intermediate levels by both dopants.

EIS analysis

In DSSCs, electron-hole recombination poses a significant challenge to device performance. Excited dye molecules contain holes which can recombine with electrons, either with the ionized

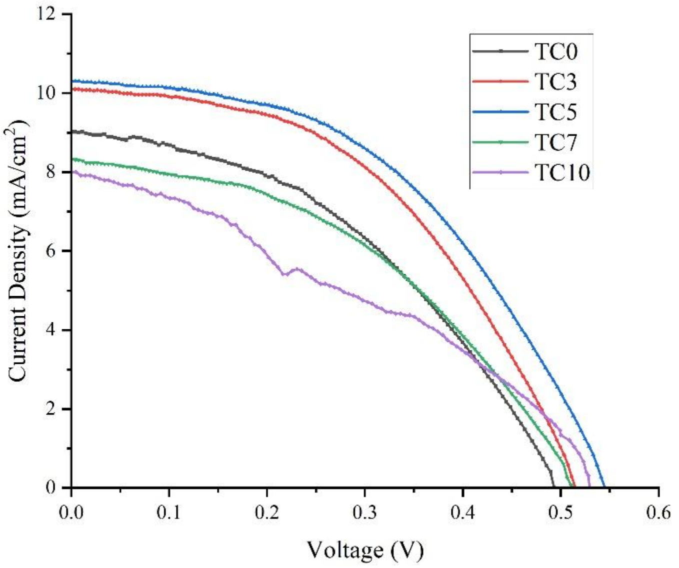

Fig. 9. J–V measurement of DSSCs based on pure and Ce-doped TiO_2 samples.

Table 4. Comparison of electrical properties obtained in this work with those reported in other studies.

Ref. Sample η (%)	Best sample η (%)	Change η (%)	Ref. Sample FF (%)	Best sample FF (%)	Synthesis method	Reference
4.45	5.62	26	43	47.4	Sol-gel	This Work (TC5)
4.45	5.44	22	43	54	Sol-gel	This Work (TN3)
4.45	6.51	46	43	67.4	Sol-gel	This Work (TN3C5)
7.2	7.65	6.25	73	72.9	Hydrothermal	[22]
1.84	2.15	17	67.6	67.9	Sol-gel	[55]
6.37	7	10	65.64	65.59	Hydrothermal	[56]
5.1	6.3	23	54	54	Ball mill	[57]
5.15	6.16	19.6	65	66	Solid state reaction	[58]
0.41	1.21	195	25.7	47	Hydrothermal	[59]

species of electrolyte or in the semiconductor matrix [60]. These charge transfer processes within the DSSC can be detected by using electrochemical impedance spectroscopy (EIS). Higher the resistance to charge recombination, higher is the cell efficiency. The radius of the

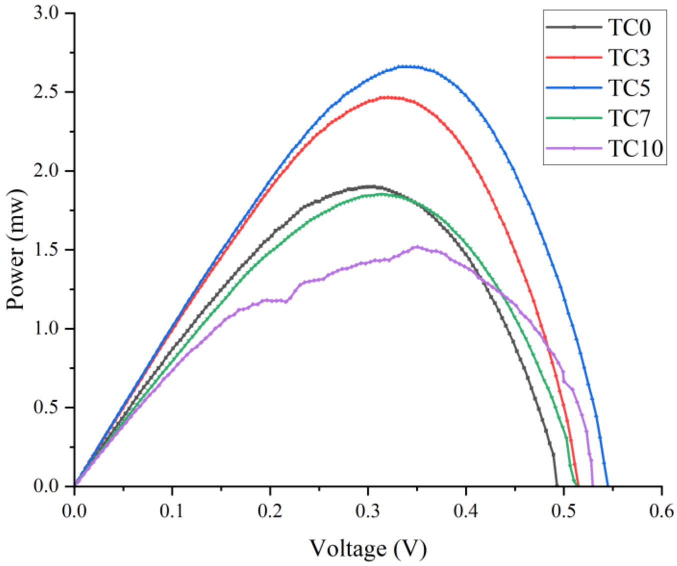

Fig. 10. Power measurement of pure and Ce-doped TiO_2 samples.

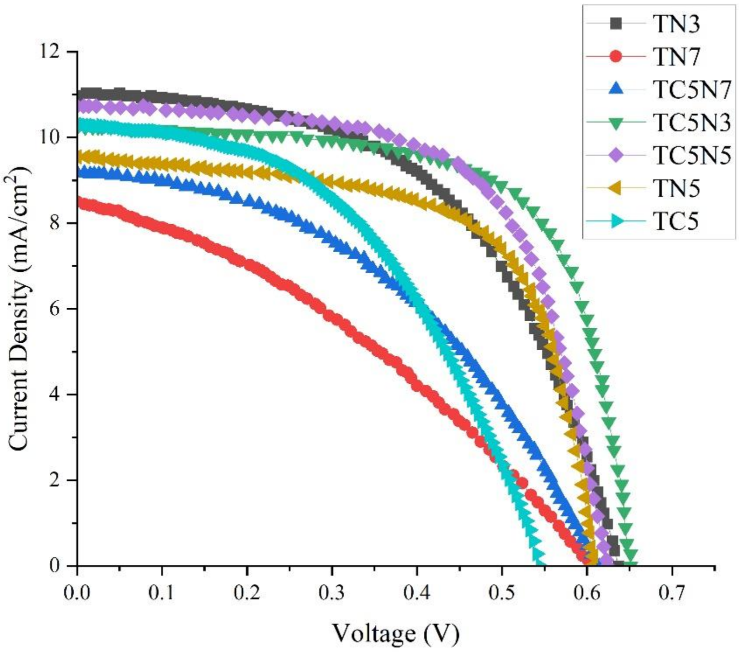

Fig. 11. J–V measurement of DSSCs based on N and N-Ce co doped TiO_2 samples.

semicircle in the impedance spectrum is indicative of the resistance to charge recombination, with a larger radius signifying lower recombination resistance [61]. EIS was employed to investigate the electron transport kinetics and internal resistance of TiO_2 films in DSSCs. The charge recombination resistance at the interface of TiO_2 and electrolyte (R3) can be determined according to impedance response. The larger semicircle observed in the low-frequency region reflects the effects of electron accumulation and transport within the TiO_2 photoanodes. In contrast, charge transfer resistance at both electrolyte/Pt counter electrode and FTO/TiO_2 interfaces (R2) can be detected by the smaller semicircle in the high-frequency region [62].

Nyquist plots, developed under short-circuit conditions at light intensities below 100 mW/cm², are presented in Fig.13. Within the frequency range of 100 kHz to 1 Hz, two distinct semicircles are observed in the complex plane plot, representing three-time constants. The corresponding parameters are summarized in Table 6. According to Fig. 13, the second semicircle of TC0 is larger than that of TC5 which indicates a decrease in R2 resistance. This reduction in interfacial resistance leads to improved efficiency and an overall decrease in internal resistance. Equation 1 is used to estimate the photoelectrons lifetime (τ_e) [63]:

$$\tau_e = 1/2\pi f_{max} \qquad (1)$$

where f_{max} is the maximum frequency of semicircle at low frequencies.

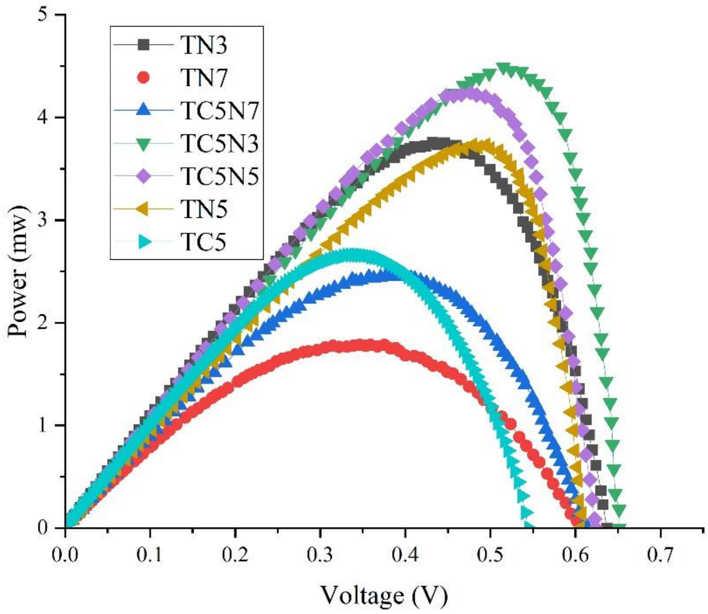

Fig. 12. Power measurement of DSSCs based on N and N-Ce co doped TiO_2 samples.

Table 5. Electrical properties of TC5, N-doped, and co-doped TiO_2 samples.

Photoanodes	N %	Ce %	J_{SC} (mA/cm^2)	V_{OC} (V)	η (%)	FF (%)
TC5	-	5%	10.30	0.545	5.613	47.4
TN3	3%	-	10.97	0.64	5.44	54
TN3C5	3%	5%	10.23	0.65	6.51	67.4
TN5	5%	-	9.55	0.606	5.41	64.5
TN5C5	5%	5%	10.73	0.62	6.14	63.29
TN7	7%	-	8.51	0.609	2.71	34.47
TN7C5	7%	7%	9.18	0.615	3.74	43.7

Fig. 14 reveals that the peak frequency increases by increasing the dopant concentration, except for TC5. This increase in frequency peak directly translates to a decrease in electron lifetime. Conversely, TC5 exhibits a significantly longer lifetime (15.23 ms), facilitating electron diffusion

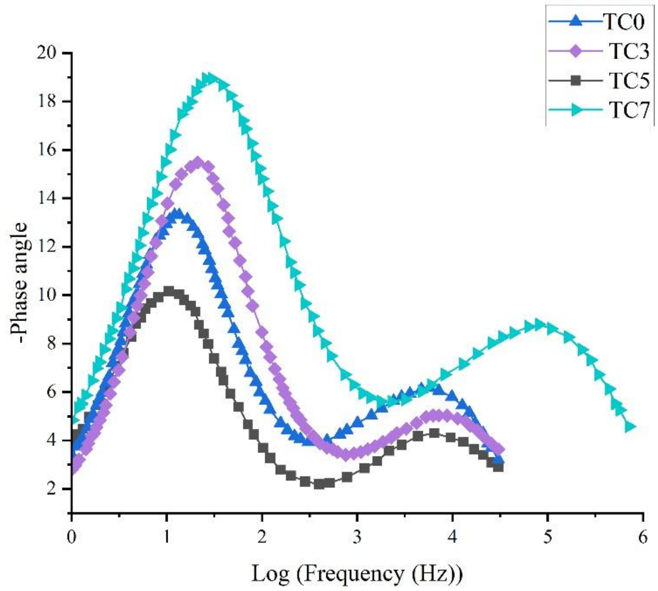

Fig. 13. Bode plots of DSSCs based on pure and Ce-doped TiO_2 samples.

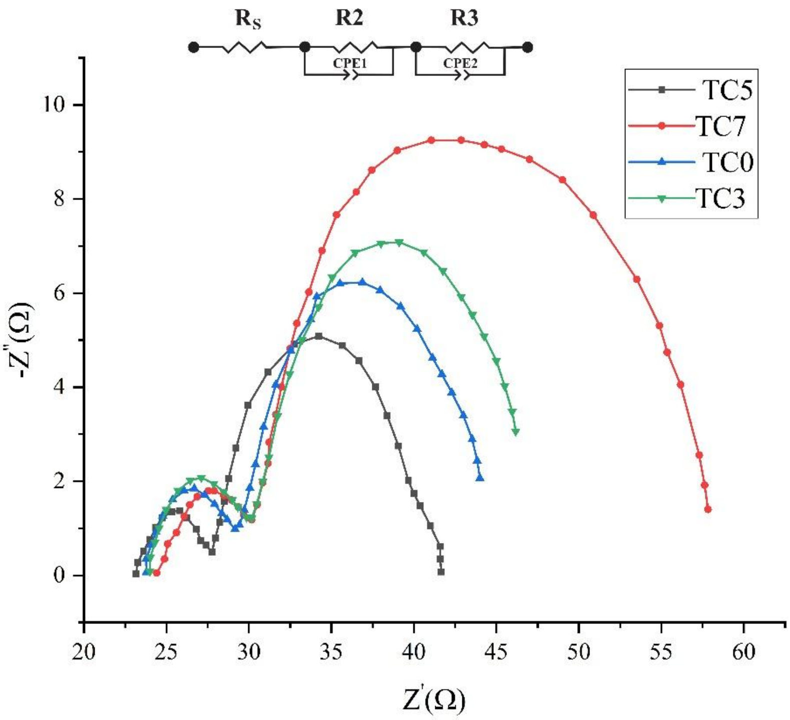

Fig. 14. EIS Nyquist plots for DSSCs based on pure and Ce-doped TiO_2 samples.

Table 6. EIS parameters of the DSSCs determined by fitting the experimental data to the equivalent circuit model.

Sample	R_S (Ω)	R_1 (Ω)	R_2 (Ω)	f_{max}	τ (ms)
TC0	23.77	5.39	14.85	12.04	13.22
TC3	23.99	6.17	16.02	21.14	7.52
TC5	23.14	4.61	13.84	10.45	15.23
TC7	24.41	5.76	27.66	30.2	5.27

and transfer due to an increase in diffusion length.

The extended electron lifetime observed in TC5 indicates a reduced recombination rate, consequently leading to higher V_{OC}. Improved electron transport in the TiO_2 after doping can be caused by a combination of factors; bandgap reduction and lattice distortions. These factors may lead to the accumulation of oxygen vacancies, thereby effectively trapping photogenerated holes. This mechanism contributes to the prolonged lifespan of both photo-excited electrons and holes [64], a finding which is consistent with the observed photovoltaic characteristics.

CONCLUSION

This study focused on the sol-gel synthesis of TiO_2 nanoparticles with different Ce concentrations and their characterization using various techniques. These nanoparticles were used for the fabrication of photoanodes and their performance in DSSCs was compared with that of N-doped and Ce,N co-doped TiO_2 photoanodes. All the synthesized samples were predominantly consisted of anatase phase, while the morphology changed from nanosheets to nanopowders upon cerium doping. The bandgap of the TiO_2 nanomaterial fell within the reported range (3.48-3.76 eV), confirming the successful bonding between Ti and Ce. Raman spectroscopy further corroborated the presence of these elemental bonds. According to PL spectra, the peak intensity increased initially at low Ce concentrations, followed by a decrease in the PL intensity by increasing the dopant concentration. Photovoltaic test of DSSC showed a 26% increase in performance for the TC5 and 46% increase for the TN3C5 compared to the TC0 sample. The electrical properties obtained for TC5, TN3, and TN3C5 samples were as follows: V_{OC} of 545 mv, 640 mv, and 650 mv, J_{sc} of 10.3 mA/cm^2, 10.97 mA/cm^2, and 10.23 mA/cm^2, FF of 47.4%, 64.5%, and 67.4%, and η of 5.613%, 5.44%, and 6.51%, respectively. EIS analysis was utilized to investigate the electron dynamics within the DSSC. The Nyquist plot revealed that the TC5 sample exhibits lower resistance, characterized by Rs of 23.14 Ω, R1 of 4.61 Ω, and R2 of 13.84 Ω, along with the longest electron lifetime recorded at 15.23 ms. This study demonstrates that co-doping of Ce and N is an effective approach for enhancing the DSSCs photovoltaic performance. The observed synergistic effect between Ce and N doping highlights the potential of this approach for developing high-efficiency, low-cost solar cells. Future studies should focus on the optimization of doping levels, examination of various co-doping strategies, and evaluation of the long-term stability of the devices.

CONFLICT OF INTEREST

The authors declare that there is no conflict of interests regarding the publication of this manuscript.

REFERENCES

1. Khan MI, Sabir M, Mustafa GM, Fatima M, Mahmood A, Abubshait SA, et al. 300 keV cobalt ions irradiations effect on the structural, morphological, optical and photovolatic properties of Zn doped TiO_2 thin films based dye sensitized solar cells. Ceram Int. 2020;46(10):16813-16819.
2. Khan MI, Farooq WA, Saleem M, Bhatti KA, Atif M, Hanif A. Phase change, band gap energy and electrical resistivity of Mg doped TiO_2 multilayer thin films for dye sensitized solar cells applications. Ceram Int. 2019;45(17):21436-21439.
3. Khan MI, Naeem M, Mustafa GM, Abubshait SA, Mahmood A, Al-Masry W, et al. Synthesis and characterization of Co and Ga co-doped ZnO thin films as an electrode for dye sensitized solar cells. Ceram Int. 2020;46(17):26590-26597.
4. O'Regan B, Grätzel M. A low-cost, high-efficiency solar cell based on dye-sensitized colloidal TiO_2 films. Nature. 1991;353(6346):737-740.
5. Gayathri V, John Peter I, Ramamanickam N, Ramachandran K. Improved performance of dye-sensitized solar cells by Cr doped TiO_2 nanoparticles. Materials Today: Proceedings. 2021;35:23-26.
6. Yang H, Yang B, Chen W, Yang J. Preparation and Photocatalytic Activities of TiO_2 -Based Composite Catalysts. Catalysts. 2022;12(10):1263.

7. Ramadhani DAK, Sholeha N, Khusna NNa, Diantoro M, Afandi AN, Osman Z, et al. Ag-doped TiO_2 as photoanode for high performance dye sensitized solar cells. Materials Science for Energy Technologies. 2024;7:274-281.
8. Ünlü B, Özacar M. Effect of Cu and Mn amounts doped to TiO_2 on the performance of DSSCs. Solar Energy. 2020;196:448-456.
9. Mehmood U, Ahmed S, Hussein IA, Harrabi K. Improving the efficiency of dye sensitized solar cells by TiO_2 -graphene nanocomposite photoanode. Photonics and Nanostructures - Fundamentals and Applications. 2015;16:34-42.
10. Mehmood U, Ahmad SHA, Al-Ahmed A, Hakeem AS, Dafalla H, Laref A. Synthesis and Characterization of Cerium Oxide Impregnated Titanium Oxide Photoanodes for Efficient Dye-Sensitized Solar Cells. IEEE Journal of Photovoltaics. 2020;10(5):1365-1370.
11. Dhonde M, Sahu K, Murty VVS, Nemala SS, Bhargava P, Mallick S. Enhanced photovoltaic performance of a dye sensitized solar cell with Cu/N Co-doped TiO_2 nanoparticles. Journal of Materials Science: Materials in Electronics. 2018;29(8):6274-6282.
12. Ma Q-l, Ma S, Huang YM. Enhanced photovoltaic performance of dye sensitized solar cell with ZnO nanohoneycombs decorated TiO_2 photoanode. Mater Lett. 2018;218:237-240.
13. Neetu, Maurya IC, Gupta AK, Srivastava P, Bahadur L. Extensive enhancement in power conversion efficiency of dye-sensitized solar cell by using Al-doped TiO_2 photoanode. J Solid State Electrochem. 2016;21(5):1229-1241.
14. De Angelis F, Fantacci S, Selloni A, Grätzel M, Nazeeruddin MK. Influence of the Sensitizer Adsorption Mode on the Open-Circuit Potential of Dye-Sensitized Solar Cells. Nano Lett. 2007;7(10):3189-3195.
15. Kamat V, Revankar V. 1,10-Phenanthroline-copper mediated ligand transformations: Synthesis and characterization of unusual mixed ligand complexes of copper (II). Inorg Chim Acta. 2018;476:77-82.
16. Roose B, Pathak S, Steiner U. Doping of TiO_2 for sensitized solar cells. Chem Soc Rev. 2015;44(22):8326-8349.
17. Tsierkezos NG, Diefenbach M, Roithová J, Schröder D, Schwarz H. Competitive Complexation of Gaseous Mn(II) by 1,10-Phenanthroline, 2,2ʹ-Bipyridine, and 4,5-Diazafluorene. Inorganic Chemistry. 2005;44(14):4969-4978.
18. Sadhu S, Poddar P. Growth of oriented single crystalline La-doped TiO_2 nanorod arrays electrode and investigation of optoelectronic properties for enhanced photoelectrochemical activity. RSC Advances. 2013;3(26):10363.
19. Maarisetty D, Baral SS. Defect-induced enhanced dissociative adsorption, optoelectronic properties and interfacial contact in Ce doped TiO_2: Solar photocatalytic degradation of Rhodamine B. Ceram Int. 2019;45(17):22253-22263.
20. Reszczyńska J, Grzyb T, Sobczak JW, Lisowski W, Gazda M, Ohtani B, et al. Visible light activity of rare earth metal doped (Er^{3+}, Yb^{3+} or Er^{3+}/Yb^{3+}) titania photocatalysts. Applied Catalysis B: Environmental. 2015;163:40-49.
21. Jafari A, Khademi S, Farahmandjou M, Darudi A, Rasuli R. Structural and Optical Properties of Ce^{3+}-Doped TiO_2 Nanocrystals Prepared by Sol–Gel Precursors. J Electron Mater. 2018;47(11):6901-6908.
22. Zhang J, Peng W, Chen Z, Chen H, Han L. Effect of Cerium Doping in the TiO_2 Photoanode on the Electron Transport of Dye-Sensitized Solar Cells. The Journal of Physical Chemistry C. 2012;116(36):19182-19190.
23. Kang SH, Kim HS, Kim J-Y, Sung Y-E. Enhanced photocurrent of nitrogen-doped TiO_2 film for dye-sensitized solar cells. Materials Chemistry and Physics. 2010;124(1):422-426.
24. Guo W, Shen Y, Wu L, Gao Y, Ma T. Effect of N Dopant Amount on the Performance of Dye-Sensitized Solar Cells Based on N-Doped TiO_2 Electrodes. The Journal of Physical Chemistry C. 2011;115(43):21494-21499.
25. Park SK, Jeong JS, Yun TK, Bae JY. Preparation of Carbon-Doped TiO_2 and Its Application as a Photoelectrodes in Dye-Sensitized Solar Cells. Journal of Nanoscience and Nanotechnology. 2015;15(2):1529-1532.
26. Subramanian A, Wang H-W. Effects of boron doping in TiO_2 nanotubes and the performance of dye-sensitized solar cells. Appl Surf Sci. 2012;258(17):6479-6484.
27. Sun Q, Zhang J, Wang P, Zheng J, Zhang X, Cui Y, et al. Sulfur-doped TiO_2 nanocrystalline photoanodes for dye-sensitized solar cells. Journal of Renewable and Sustainable Energy. 2012;4(2).
28. Yang S, Guo S, Xu D, Xue H, Kou H, Wang J, et al. Improved efficiency of dye-sensitized solar cells applied with F-doped TiO_2 electrodes. Journal of Fluorine Chemistry. 2013;150:78-84.
29. Madurai Ramakrishnan V, Natarajan M, Pitchaiya S, Santhanam A, Velauthapillai D, Pugazhendhi A. Microwave assisted solvothermal synthesis of quasi cubic F doped TiO_2 nanostructures and its performance as dye sensitized solar cell photoanode. International Journal of Energy Research. 2020;45(12):17259-17268.
30. Rajaramanan T, Kumara GRA, Velauthapillai D, Ravirajan P, Senthilnanthanan M. Ni/N co-doped P25 TiO_2 photoelectrodes for efficient Dye-Sensitized Solar Cells. Mater Sci Semicond Process. 2021;135:106062.
31. Balachandran K, Kalaivani T, Thangaraju D, Mageswari S, Viswak Senan MS, Preethi A. Fabrication of photoanodes using sol-gel synthesized Ag-doped TiO_2 for enhanced DSSC efficiency. Materials Today: Proceedings. 2021;37:515-521.
32. Cheng Y, Zhang M, Yao G, Yang L, Tao J, Gong Z, et al. Band gap manipulation of cerium doping TiO_2 nanopowders by hydrothermal method. J Alloys Compd. 2016;662:179-184.
33. Unal FA, Ok S, Unal M, Topal S, Cellat K, Şen F. Synthesis, characterization, and application of transition metals (Ni, Zr, and Fe) doped TiO_2 photoelectrodes for dye-sensitized solar cells. J Mol Liq. 2020;299:112177.
34. Lee JY, Choi J-H. Sonochemical Synthesis of Ce-doped TiO_2 Nanostructure: A Visible-Light-Driven Photocatalyst for Degradation of Toluene and O-Xylene. Materials (Basel, Switzerland). 2019;12(8):1265.
35. Venkatachalam N, Palanichamy M, Murugesan V. Sol–gel preparation and characterization of alkaline earth metal doped nano TiO_2: Efficient photocatalytic degradation of 4-chlorophenol. J Mol Catal A: Chem. 2007;273(1-2):177-185.
36. Khannam M, Sharma S, Dolui S, Dolui SK. A graphene oxide incorporated TiO_2 photoanode for high efficiency quasi solid state dye sensitized solar cells based on a poly-vinyl alcohol gel electrolyte. RSC Advances. 2016;6(60):55406-55414.
37. Hirian R, Pop V, Isnard O, Benea D. Magnetic Properties of (Fe,Co)5SiB2 Alloys by W Doping. Studia Universitatis Babeș-Bolyai Physica. 2022:25-33.
38. Chen Q, Jiang D, Shi W, Wu D, Xu Y. Visible-light-activated

Ce–Si co-doped TiO_2 photocatalyst. Appl Surf Sci. 2009;255(18):7918-7924.

39. Yu J, Low J, Xiao W, Zhou P, Jaroniec M. Enhanced Photocatalytic CO_2 Reduction Activity of Anatase TiO_2 by Coexposed {001} and {101} Facets. Journal of the American Chemical Society. 2014;136(25):8839-8842.
40. Lee M, Kim M-S, Oh J-M, Park JK, Paek S-M. Hybridization of Layered Titanium Oxides and Covalent Organic Nanosheets into Hollow Spheres for High-Performance Sodium-Ion Batteries with Boosted Electrical/Ionic Conductivity and Ultralong Cycle Life. ACS Nano. 2023;17(3):3019-3036.
41. Ako RT, Ekanayake P, Young DJ, Hobley J, Chellappan V, Tan AL, et al. Evaluation of surface energy state distribution and bulk defect concentration in DSSC photoanodes based on Sn, Fe, and Cu doped TiO_2. Appl Surf Sci. 2015;351:950-961.
42. Delekar SD, Yadav HM, Achary SN, Meena SS, Pawar SH. Structural refinement and photocatalytic activity of Fe-doped anatase TiO_2 nanoparticles. Appl Surf Sci. 2012;263:536-545.
43. Dey S, Roy SC. Influence of Ce doping on morphology, crystallinity and photoelectrochemical charge transfer characteristics of TiO_2 nanorod arrays grown on conductive glass substrate. J Alloys Compd. 2021;881:160481.
44. Raguram T, Rajni KS. Effect of Ni doping on the characterization of TiO_2 nanoparticles for DSSC applications. Journal of Materials Science: Materials in Electronics. 2021;32(13):18264-18281.
45. Fu C, Li T, Qi J, Pan J, Chen S, Cheng C. Theoretical study on the electronic and optical properties of Ce^{3+}-doped TiO_2 photocatalysts. Chem Phys Lett. 2010;494(1-3):117-122.
46. Fazil M, Ahmad T. Pristine TiO_2 and Sr-Doped TiO_2 Nanostructures for Enhanced Photocatalytic and Electrocatalytic Water Splitting Applications. Catalysts. 2023;13(1):93.
47. Baruah M, Ezung SL, Sharma S, Bora Sinha U, Sinha D. Synthesis and characterization of Ni-doped TiO_2 activated carbon nanocomposite for the photocatalytic degradation of anthracene. Inorg Chem Commun. 2022;144:109905.
48. Liu Y, Fang P, Cheng Y, Gao Y, Chen F, Liu Z, et al. Study on enhanced photocatalytic performance of cerium doped TiO_2 -based nanosheets. Chem Eng J. 2013;219:478-485.
49. Martin MV, Alfano OM, Satuf ML. Cerium-doped TiO_2 thin films: Assessment of radiation absorption properties and photocatalytic reaction efficiencies in a microreactor. Journal of Environmental Chemical Engineering. 2019;7(6):103478.
50. Liqiang J, Yichun Q, Baiqi W, Shudan L, Baojiang J, Libin Y, et al. Review of photoluminescence performance of nano-sized semiconductor materials and its relationships with photocatalytic activity. Sol Energy Mater Sol Cells. 2006;90(12):1773-1787.
51. Yang L, Zhang Y, Ruan W, Zhao B, Xu W, Lombardi JR. Improved surface-enhanced Raman scattering properties of TiO_2 nanoparticles by Zn dopant. J Raman Spectrosc. 2010;41(7):721-726.
52. Physical Mechanism Behind Enhanced Photoelectrochemical and Photocatalytic Properties of Superhydrophilic Assemblies of 3D- TiO_2 Microspheres with Arrays of Oriented, Single-Crystalline TiO_2 Nanowires as Building Blocks Deposited on Fluorine-Doped Tin Oxide. American Chemical Society (ACS).
53. M MAS, N K, K R, K S, S MB, R RB, et al. Influence of heat treatment on the properties of hydrothermally grown 3D/1D TiO_2 hierarchical hybrid microarchitectures over TiO_2 seeded FTO substrates. Appl Surf Sci. 2018;449:122-131.
54. Gao Y, Xu J, Shi S, Dong H, Cheng Y, Wei C, et al. TiO_2 Nanorod Arrays Based Self-Powered UV Photodetector: Heterojunction with NiO Nanoflakes and Enhanced UV Photoresponse. ACS Applied Materials and Interfaces. 2018;10(13):11269-11279.
55. Khan MI, Suleman A, Hasan MS, Ali SS, Al-Muhimeed TI, AlObaid AA, et al. Effect of Ce doping on the structural, optical, and photovoltaic properties of TiO_2 based dye-sensitized solar cells. Materials Chemistry and Physics. 2021;274:125177.
56. Xing G, Zhang Z, Qi S, Zhou G, Zhang K, Cui Z, et al. Effect of cerium ion modifications on the photoelectrochemical properties of TiO_2 -based dye-sensitized solar cells. Opt Mater. 2018;75:102-108.
57. Lee JW, Cho W-H, Dhayal M, Park KH. Short Communication: Cerium Doped Fluorescence into TiO_2 Photoelectrode for Enhancement of Electrochemical Response in Dye Sensitized Solar Cells. International Journal of Electrochemical Science. 2015;10(10):8236-8242.
58. Rajaramanan T, Heidari Gourji F, Velauthapillai D, Ravirajan P, Senthilnanthanan M. Enhanced Photovoltaic Properties of Dye-Sensitized Solar Cells through Ammonium Hydroxide-Modified (Nitrogen-Doped) Titania Photoanodes. International Journal of Energy Research. 2023;2023:1-12.
59. Mousa MA, Khairy M, Mohamed HM. Dye-Sensitized Solar Cells Based on an N-Doped TiO_2 and TiO_2 -Graphene Composite Electrode. J Electron Mater. 2018;47(10):6241-6250.
60. Ondersma JW, Hamann TW. Recombination and redox couples in dye-sensitized solar cells. Coord Chem Rev. 2013;257(9-10):1533-1543.
61. Hosseinnezhad M, Gharanjig K, Rouhani S, Imani H, Razani N. Environmentally Dyeing Using Dried Walnut Husk as Bio-Mordant: Investigation of Creating New Red and Yellow Shades on Wool. Journal of Natural Fibers. 2021;19(15):10953-10963.
62. Zhao Z, Liu Q. Effects of lanthanide doping on electronic structures and optical properties of anatase TiO_2 from density functional theory calculations. J Phys D: Appl Phys. 2008;41(8):085417.
63. Kern R, Sastrawan R, Ferber J, Stangl R, Luther J. Modeling and interpretation of electrical impedance spectra of dye solar cells operated under open-circuit conditions. Electrochimica Acta. 2002;47(26):4213-4225.
64. Kim YJ, Lee MH, Kim HJ, Lim G, Choi YS, Park NG, et al. Formation of Highly Efficient Dye-Sensitized Solar Cells by Hierarchical Pore Generation with Nanoporous TiO_2 Spheres. Adv Mater. 2009;21(36):3668-3673.